Thermal Environment of Transatmospheric Vehicles

Michael E. Tauber*
NASA Ames Research Center, Moffett Field, California
and
Henry G. Adelman†
Eloret Institute, Sunnyvale, California

A transatmospheric vehicle using primarily airbreathing propulsion must fly in the denser part of the atmosphere to achieve adequate acceleration to reach orbital speed. The potentially long ascent times, combined with the need for a relatively sharp nose and wing leading edges for low drag, result in a severe aerothermodynamics environment. The ascent peak stagnation point and equilibrium wall temperatures for the wing leading edge can reach values of 4000 and 3000 K, respectively, for high-dynamic-pressure trajectories, making some form of active cooling mandatory. The corresponding temperatures during entry are about 1500 K lower. The vehicle windward centerline temperatures are more moderate, however, with values peaking around 1500 K. Therefore, radiative cooling should be effective over large areas of the vehicle. The windward centerline heat loads are relatively insensitive to the dynamic pressure of the ascent trajectory, in contrast to the stagnation point and wing leading edge. The windward surface entry heat loads are much lower, but depend strongly on the flight path.

Nomenclature

A = reference area of entry vehicle
a = acceleration
C = see Eq. (13)
C_D = drag coefficient
C_L = lift coefficient
D = drag
g = acceleration of gravity
g_w = ratio of wall enthalpy to total enthalpy
I = specific impulse
K = constant, Eq. (12b)
L = lift
m = vehicle mass
Q = total heat load per unit area
q = dynamic pressure
$\dot{q}$ = heat-transfer rate into the body per unit area
R_0 = planetary radius
r_n = body nose radius
T = thrust
T_w = equilibrium wall temperature
t = time
V = flight velocity
V_f = final velocity at end of heating pulse
V_s = surface grazing (circular) satellite speed (7.9 km/s)
x = distance measured along body surface
α = angle of attack
Δ = sweep angle of wing leading edge
γ = specific heat ratio
γ_f = flight-path angle
ϵ = surface emissivity
β = inverse atmospheric density scale height
ρ = freestream density
ρ_0 = sea-level atmospheric density
ϕ = bank angle
θ = local body angle with respect to freestream
σ = Stefan-Boltzmann constant

Subscripts

FP = flat plate
f = fuel
i = initial value
LE = wing leading edge
max = maximum
w = wall
0 = stagnation point
1 = laminar boundary layer
2 = turbulent boundary layer

Received April 20, 1987; presented as Paper 87-1514 at the AIAA 22nd Thermophysics Conference, Honolulu, Hawaii, June 8-10, 1987; revision received July 6, 1987.

*Research Scientist. Associate Fellow AIAA.
†Research Scientist. Member AIAA.

Introduction

THE need for more economical access to space has spurred renewed interest in transatmospheric vehicles (TAVs) in both the United States and in Europe. Such TAVs would have responsive, flexible operational characteristics approaching those of aircraft and might eventually replace the Shuttle by providing short launch notice and turnaround times. The TAV would be able to take off and land from ordinary runways and operate in low-Earth orbits.

The configurations proposed for TAVs would use primarily airbreathing propulsion systems for extended periods of hypervelocity flight to orbital speed. Hypervelocity flight within the atmosphere subjects the vehicle to severe aerodynamic heat fluxes and total heat loads. Therefore, the thermal protection of such vehicles will be major design considerations. In a previous paper,[1] the authors presented the results of parametric heating calculations for approximate ascent trajectories and for atmospheric entries. Even the approximate calculations[1] showed that ascent trajectory heating determined the thermal protection requirements. To effectively study the critical ascent heating environments, however, the propulsion and aerodynamic performance of the vehicles must also be approximated. From the performance characteristics, angle-of-attack histories can be derived that allow more meaningful computation of the windward lifting surface heating rates and heat loads. The present paper contains a parametric analysis of atmospheric flight trajectories and the accompanying heating experienced at several key body loca-

tions. The heating rates, equilibrium wall temperatures, and total heat loads at the stagnation point, along a postulated wing leading edge and on the windward bottom surface centerline of the vehicle, will be presented.

Performance Analysis

Rocket-launched space vehicles such as the Shuttle Orbiter experience relatively little aerodynamic heating during launch. The large thrust available during ascent results in passage through the sensible atmosphere in a matter of minutes. Burnout velocity is reached at very high altitudes where the aerodynamic heating is low. For example, the time-integrated heating (total heat load) at the Shuttle Orbiter nose stagnation point is almost two orders of magnitude less during launch than during atmospheric entry. In contrast, a vehicle using an airbreathing propulsion system must fly a long time in the denser portion of the atmosphere to develop sufficient thrust to accelerate to orbital speed. The extended period of hypervelocity atmospheric flight exposes the vehicle to high local heating rates and large total heating loads. To determine the thermal environments of the TAV, it is necessary to model the ascent flight paths and angle-of-attack histories as well as the entry trajectories to calculate the heating at selected body locations. This formulation will be performed in the following sections.

Trajectories

For the ascent, a group of representative trajectories are defined. The objective is to determine flight paths that can be parametrically varied, but are generally applicable for airbreathing powerplants, without having to specify details such as engine cycles, efficiencies, and so on. For the atmospheric entry, the equilibrium glide trajectory[2] is stipulated. The equilibrium glide flight path is flown by manned vehicles that are returning from near-Earth orbit and that have adequate lift, since the path affords low decelerations.

The entire ascent trajectory consists of a number of segments beginning with takeoff, then a subsonic climb, acceleration through the high-drag transonic regime to supersonic speed, followed typically by a hypersonic climb to high altitude. From the standpoint of heating, only hypersonic flight is of major concern. It is assumed here that the hypersonic flight segment is a constant dynamic pressure climb[3] so that

$$\tfrac{1}{2}\rho V^2 = q \tag{1}$$

where q is constant. If the engine thrust axis is aligned with the body axis, the equation of motion along the flight path is

$$m\frac{dV}{dt} = T\cos\alpha - D - W\sin\gamma_f \tag{2}$$

where T is the thrust and γ_f the flight-path angle. By assuming an exponential density variation with altitude y, where ρ_0 is the sea level density and $1/\beta$ the atmospheric density scale height,

$$\rho = \rho_0 e^{-\beta y} \tag{3}$$

the flight-path angle for a constant-dynamic-pressure climb can be easily calculated. Combining Eqs. (1) and (3) with the kinematic relation

$$V\sin\gamma_f = \frac{dy}{dt} \tag{4}$$

yields

$$\sin\gamma_f = \frac{2}{\beta V^2}\frac{dV}{dt} \tag{5}$$

It can be seen from Eq. (5) that γ_f becomes small at high speeds. For example, since the scale height is about 7.2 km at high altitudes, for an acceleration of 2 m/s^2 and a speed of 4 km/s, the flight-path angle is 0.1 deg. Therefore, the last term on the right-hand side of Eq. (2) can be neglected at high speeds. Since the hypersonic part of the flight regime dominates the entire trajectory and if it is assumed that the drag coefficient is approximately constant at high speeds, then the drag is also approximately constant if dynamic pressure does not vary. Now, Eq. (2) becomes, for $\alpha \ll 1$,

$$\frac{dV}{dt} = \frac{T}{m} - \frac{D}{m} \tag{6}$$

The thrust T can be a function of many factors, including the type of powerplant, flight speed, and altitude. However, to make the present analysis as general as possible, it is assumed that $T/m - D/m$ is approximately constant, so that the climb occurs at a constant acceleration

$$\frac{dV}{dt} \approx a \tag{7}$$

Therefore, two parameters are available to vary the high-speed portion of the ascent trajectory. The first is the dynamic pressure, which determines the flight altitude. The second parameter is the average (constant) value of the acceleration, which defines the flight time to reach a given speed; therefore, the time is independent of the trajectory flown.

Propulsion

A general expression for the thrust at any time is

$$T = -gI\frac{dm}{dt} \tag{8}$$

where I is the propulsion system's specific impulse in seconds. Combining Eqs. (6–8) yields

$$\frac{dV}{a} = -gI\frac{dm}{ma + D} \tag{9}$$

Assuming that an average constant value of specific impulse can be defined permits Eq. (9) to be readily integrated to find the fuel fraction m_f/m_i required to reach orbital speeds V_s,

$$\frac{1}{a}\int_0^{V_s} dV = -gI_{av}\int_{m_i}^{m_i - m_f}\frac{dm}{ma + D} \tag{10a}$$

and

$$\frac{m_f}{m_i} = \left(1 + \frac{C_D A}{m_i}\frac{q}{a}\right)(1 - e^{-I_{av}/gV_s})$$

$$= (1 + C_0)(1 - e^{-I_{av}/gV_s}) \tag{10b}$$

Note that the dimensionless ratio C_0 contains the wing loading m_i/A, the dynamic pressure, and the acceleration. [Note that for $C_0 = 0$, which corresponds to $C_D = 0$, Eq. (10b) becomes the familiar rocket equation for flight without atmospheric drag.] The required average specific impulse is shown as a function fuel fraction in Fig. 1. A vehicle fuel fraction of at least 0.6 is required if the average specific impulse is about 1500 s. The influence of the aerodynamic parameter $m_i/C_D A$ and the dynamic pressure of the trajectory q on fuel fraction is also apparent.

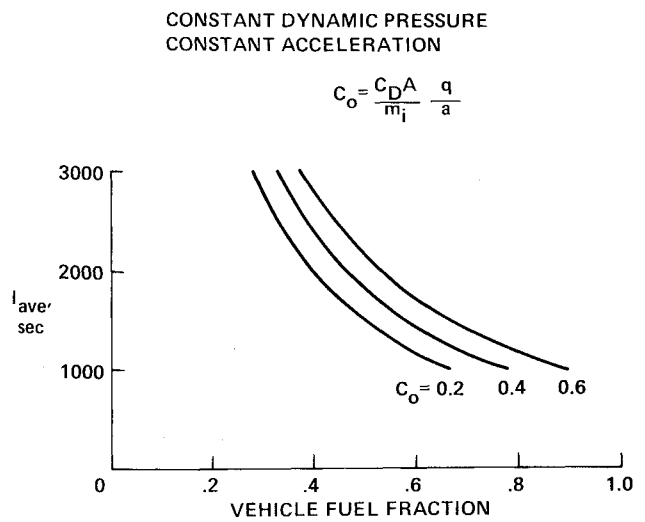

Fig. 1 Required specific impulse as function of fuel fraction (constant dynamic pressure and acceleration).

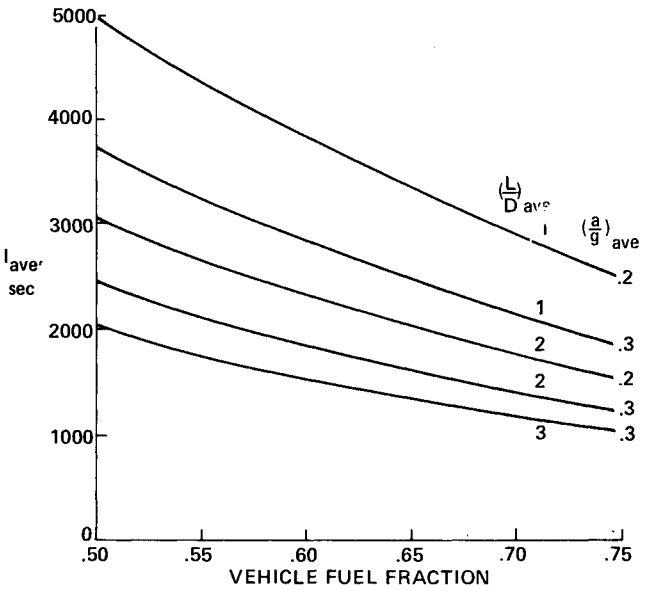

Fig. 2 Required specific impulse as function of fuel fraction and performance.

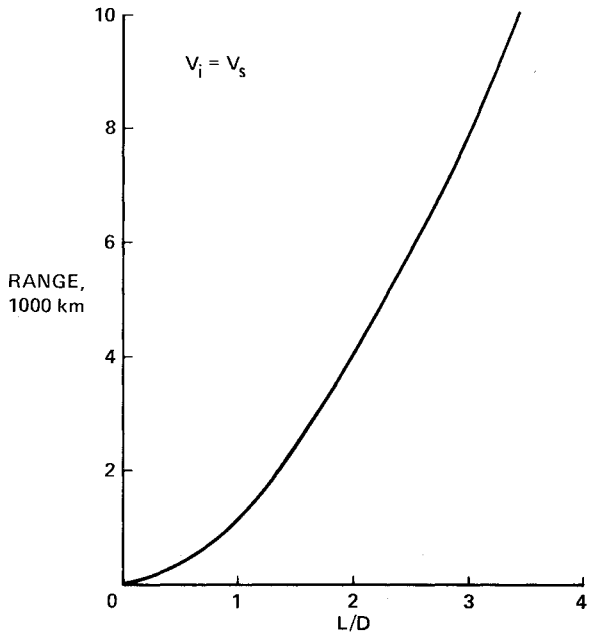

Fig. 3 Variation of maximum lateral range with L/D.

Aerodynamics

It is now possible to estimate the aerodynamic lift requirements for transatmospheric flight. For a shallow flight-path angle, the lift is

$$L = mg - T\sin\alpha - (mV^2/R_0) \tag{11a}$$

Here the right-hand term is the centrifugal force that equals the weight when satellite speed V_s is reached. For small angles of attack, Eq. (11a) can be rewritten as

$$D = \frac{mg}{L/D}\left(1 - \frac{V^2}{gR_0}\right) = \frac{mg}{L/D}\left(1 - \frac{V^2}{V_s^2}\right) \tag{11b}$$

and substituting Eq. (11b) into Eq. (9) gives

$$-gI\frac{dm}{m} = \left[1 + \frac{1}{(a/g)(L/D)}\left(1 - \frac{V^2}{V_s^2}\right)\right]dV \tag{12}$$

Assuming that L/D and the specific impulse can be represented by average values that are constant at hypersonic speeds permits integration of Eq. (12) and yields

$$\frac{m_f}{m_i} = 1 - \exp\left[-\frac{V_s}{gI_{av}}\left(1 + \frac{2}{3(a/g)(L/D)_{av}}\right)\right] \tag{13}$$

The result of plotting Eq. (13) is shown in Fig. 2. Using the approximate previous vlaues of $I_{ave} = 1500$ s and $m_f/m_i = 0.6$ in Fig. 2 indicates that an average L/D in the neighborhood of 2-3 is required at an average acceleration of 0:3 g. For comparison, the hypersonic maximum lift/drag ratio of the Shuttle is about 2.[4]

Maneuvering and Entry

Since a major objective of the TAV is the ability to operate from many bases, such vehicles require a large lateral range. The maximum lateral range upon reentering the atmosphere is proportional to the peak[5] L/D and is shown in Fig. 3. For instance, a maximum lift/drag ratio of 2.5 affords a lateral range of up to 6000 km. (A global choice of landing sites corresponds to a cross-range of 10,000 km and requires an L/D of 3.4.) However, such large lateral or longitudinal distances are achieved only at the expense of long heating pulses (as will be shown), since the flight time is directly proportional to L/D. The total laminar heat load, however, is proportional to the square root of L/D.[6]

For longitudinal flight, modest lift/drag ratios are adequate. An L/D on the order of one-half, or greater, permits the vehicle to fly an equilibrium glide trajectory upon atmospheric entry. The primary advantages of such a shallow trajectory are moderate heating rates and low deceleration forces. (The peak deceleration during Shuttle entry is about 1.6 g.) The low decelerations are advantageous for the crew and also make light structures possible.

The flight-path expression for the equilibrium glide path comes directly from equating the difference between the lift and weight to the centrifugal force[2]

$$L - mg = -mV^2/R_0 \tag{14a}$$

where R_0 is the Earth's radius. This equation gives

$$\frac{\rho V^2}{V_s^2 - V^2} = \frac{2}{R_0}\frac{m}{C_L A} = K \tag{14b}$$

where V_s is the circular satellite speed and the right-hand side can be considered constant during the high-speed por-

tion of the entry. If the vehicle is banked during entry, as is done with Shuttle to reduce the duration of the heating pulse, then

$$C_L = C_{L_0} \cos\phi$$

where C_{L_0} is the lift coefficient at zero bank angle.

Aerodynamic Heating Analysis

Basic Equations

It is assumed that the heating rate per unit area can be written in the form

$$\dot{q} = C\rho^N V^M \tag{15}$$

where N and M can be assumed constant. The form of Eq. (15) applies in the flight regime where boundary-layer theory is valid and the flowfield is in equilibrium. Equation (15) is a good approximation for both laminar[7,8] and turbulent[9] convection at a fully catalytic surface in the absence of boundary-layer mass addition. The numerical values used in Eq. (15) are from Refs. 7–9; none have been modified using Shuttle, or other, flight data. However, the expression derived in Ref. 8 for laminar flat-plate heating was slightly simplified. (Values of N, M, and C are listed in the Appendix.) Assuming a fully catalytic wall for laminar boundary layers is conservative and makes Eq. (15) independent of the choice of heat shielding material. Since C is a weak function of wall temperature, which for radiative equilibrium is given by

$$T_w = (\dot{q}/\epsilon\sigma)^{1/4} \tag{16}$$

it is necessary to iterate between Eqs. (15) and (16) to find the heating rate.

The form of Eq. (15) is suitable for calculating the stagnation point or the flat-plate heat transfer. The wing leading-edge heating was computed using the swept-cylinder theory[10] in the form

$$\dot{q}_{LE} = [\tfrac{1}{2}(\dot{q}_0)^2 \cos^2\Delta + (\dot{q}_{FP})^2 \sin^2\Delta]^{1/2}(\cos\alpha) \tag{17}$$

where Δ is the leading-edge sweep angle.

The beginning of boundary-layer transition from laminar to turbulent flow is predicted using a modified correlation of local length Reynolds number and local Mach number.[11] The original correlation for cones, shown in Ref. 11, was modified and extended to nonaxisymmetric bodies by adding transition data from Shuttle flights.[12,13] The length of the transitional boundary-layer region is assumed to be the same as the preceding laminar flow distance. A linear variation is assumed between the laminar values and the fully established, turbulent heating rates. Comparisons of laminar, transitional, and turbulenty heating rates with Shuttle flight data will be presented next.

Comparison with Flight Data

The STS-1 and STS-2 flight centerline heating rates, determined from temperature measurements,[13,14] are compared with calculations at six flight conditions in Fig. 4. The laminar and turbulent flat plate versions of Eq. (15) were used. The STS-2 flight conditions shown in Fig. 4a cover the high-speed, high-altitude laminar boundary-layer regime. The agreement between measured and calculated heating rates is better over the forward portion of the vehicle than over the aft part, where the flight values are substantially higher and do not exhibit the $x^{-1/2}$ decrease with distance characteristic of an undisturbed laminar boundary layer. (Chemical nonequilibrium and reduced wall catalycity may be responsible.[14,15]) However, at the lower speeds and altitudes where the STS-1 measurements were made, catalytic

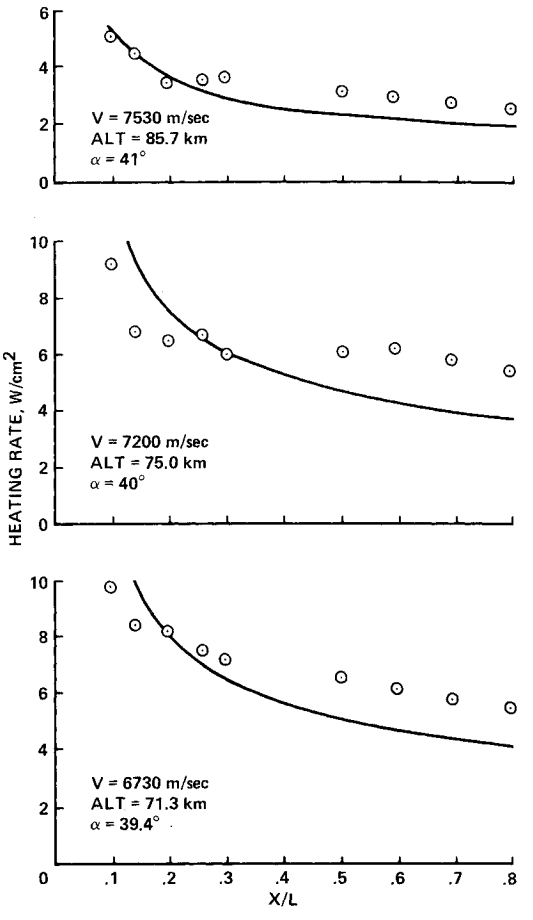

a) STS-2

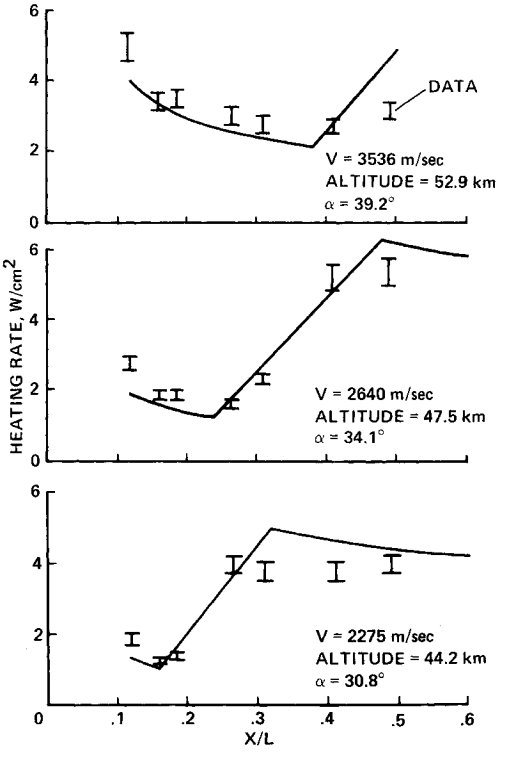

b) STS-1

Fig. 4 Comparison of centerline heating calculations with flight data.

wall effects were negligible. Note that laminar, transitional, and turbulent boundary-layer heating are clearly evident in Fig. 4b. (The error bars represent uncertainties in the surface emissivity.[13]) The high-entropy gas layer generated by the Shuttle's blunt nose substantially increases the laminar heating near $X/L=0.1$ at the flight conditions shown in Fig. 4b, where the flow should be in equilibrium. However, the much sharper nose of a TAV should largely eliminate the high-entropy layer, and the flat-plate approximation should yield more reasonable laminar heat-transfer values. The fully turbulent heating predictions are somewhat too high, which is typical for a method based on reference enthalpy. The comparisons shown in Fig. 4 cover an atmospheric density range of 300, while the flight speeds varied by a factor of 3.3. In view of the simplified nature of the present analysis, the overall agreement is considered good.

Next, expressions for the heating rates and total heat loads during ascent and entry will be formulated. Since detailed derivations are given in Refs. 1 and 6, the presentation of the heating calculations over the trajectories will be brief.

Ascent

The heating rate per unit area during the hypersonic climb at a constant dynamic pressure is found by substituting Eq. (1) into Eq. (15)

$$\dot{q}=C(2q)^N V^{M-2N} \tag{18}$$

where q is the dynamic pressure. The total heat load per unit area is determined by integrating Eq. (18) using Eq. (7)

$$Q=\frac{1}{a}\int_{V_1}^{V_2} C(2q)^N V^{M-2N}\,\mathrm{d}V \tag{19}$$

Both the dynamic-pressure term and C are functions of velocity; the first is because N changes if transition occurs, while C is weakly dependent on the total enthalpy and wall temperature.

Entry

The heating rate per unit area during entry is determined by combing Eq. (14b) with Eq. (15) and is

$$\dot{q}=CK^N(V_s^2-V^2)^N V^{M-2} \tag{20}$$

The expression for the peak heating rate is[6]

$$\dot{q}_{\max}=C(2NK)^N(V_s/\sqrt{M})^M(M-2N)^{M/2-N} \tag{21a}$$

or, in terms of vehicle parameters only

$$\dot{q}_{\max}\sim(m/C_L A)^N \tag{21b}$$

The general expression for the total heat load per unit area is[6]

$$Q=\frac{2m}{C_D A}\int_{V_f}^{V_i} CK^{N-1}(V_s^2-V^2)^{N-1}V^{M-2N}\mathrm{d}V \tag{22}$$

In regions of the vehicle that experience only laminar heating, the total heating is approximately

$$Q\approx C_1 K^{-1/2} V_s^2 \frac{m}{C_D A} \tag{23a}$$

After substituting for K, this gives the proportionality

$$Q\sim\left(\frac{m}{C_D A}\frac{L}{D}\right)^{1/2} \tag{23b}$$

The heating penalties associated with high L/D entry flight paths, for either long longitudinal or lateral distances, are apparent from Eq. (23b).

Study Parameters

It is intended to make the study general without defining a detailed vehicle configuration and specific missions. The ascent parameters to be studied consist of a family of hypersonic climb flight paths accelerating to a speed of about 8 km/s. The vehicle can then coast to higher altitudes or out of the atmosphere. The coast phase is analyzed in Ref. 16. Subsequently, the vehicle reenters the atmosphere along one of a series of equilibrium glide trajectories and the analysis is resumed.

Vehicle Characteristics

It is desirable to avoid using a specific vehicle configuration; however, the extended period of hypersonic flight required to achieve orbital velocity within the atmosphere mandates low-drag shapes. To reduce the number of parameters, the following geometric assumptions are made. The bottom surface of the vehicle is taken to be approximately flat. The radius of the vehicle's nose is taken as 10 cm. The wing leading edge is assumed to be swept back at 75 deg with a radius that varies linearly from 9 cm at the wing root to 3 cm at a point 15 m along the leading edge.

Trajectories

The hypersonic part of the climb trajectories, when heating is large, is assumed to occur at constant dynamic pressures of 0.2, 0.4, and 0.8 atm [Eq. (18)]. The average accelerations during the climbs are assumed to be constant at values of 0.2–0.8 g [Eq. (19)]. Only a limited number of equilibrium glide entry trajectories [Eq. (14)] will be considered. The glide paths will be calculated for lift/drag ratios of 1.2 and 1.8.

Aerodynamics

The aerodynamic histories of the constant dynamic pressure climbs are determined by combining Eqs. (1), (2), and (11a) to yield an expression in terms of lift and drag coefficients

$$C_L + C_D\tan\alpha=\left(\frac{m_i g}{Aq}\right)\left(\frac{m}{m_i}\right)\left[\left(1-\frac{V^2}{V_s^2}\right)-\left(\frac{1}{g}\frac{\mathrm{d}V}{\mathrm{d}t}+\sin\gamma_f\right)\tan\alpha\right] \tag{24}$$

The lift and drag can be related to angle of attack at high Mach numbers by

$$C_L=(\gamma+1)\sin^2\alpha\cos\alpha \tag{25a}$$

$$C_D=(\gamma+1)\sin^3\alpha+C_{D_0} \tag{25b}$$

The relations in Eqs. (25) come from hypersonic small-disturbance theory[17] and Newtonian impact theory. In evaluating Eqs. (25), an estimated local shock layer value of γ was used. Below Mach 10, where lift coefficient becomes a function of both α and α^2, Refs. 4 and 18 were used as a guide to modify Eq. (25a). Equations (24) and (25) are a set of three parametric equations in the three unknowns, C_L, C_D, and α. The parameters are dynamic pressure, average acceleration, and wing loading. However, when the angle of attack is small, the second term on the right-hand side of Eq. (24) becomes small and the force coefficients become insensitive to acceleration. Therefore, the trajectory depends primarily on the dynamic pressure.

The lift coefficients and corresponding angles of attack are shown in Fig. 5 as a function of speed for constant dynamic pressure flight paths of 0.2, 0.4, and 0.8 atm. A wing

loading of 500 kg/m^2 has been assumed. Now the heating can be computed for the chosen trajectories.

Results

The parameters described are now used to calculate the heating rates, equilibrium wall temperatures (for $\epsilon = 0.8$), and total heating loads at the vehicle's nose stagnation point, on the wing leading edge, and along the bottom surface centerline. Heating at all three body locations will be illustrated for the three ascent trajectories. Since the entry heating is extensively discussed in Ref. 1 and is also less severe, the ascent heating will be emphasized here.

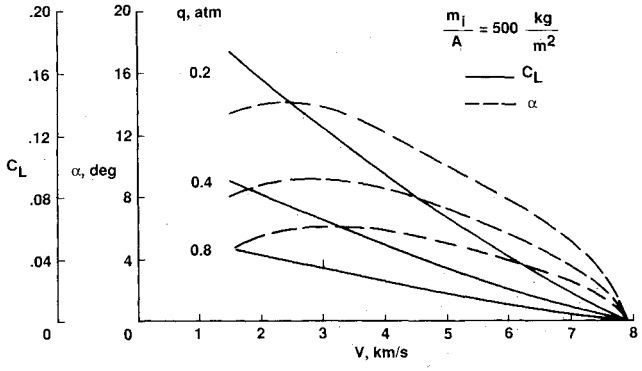

Fig. 5 Variation of lift coefficient and angle of attack with flight speed.

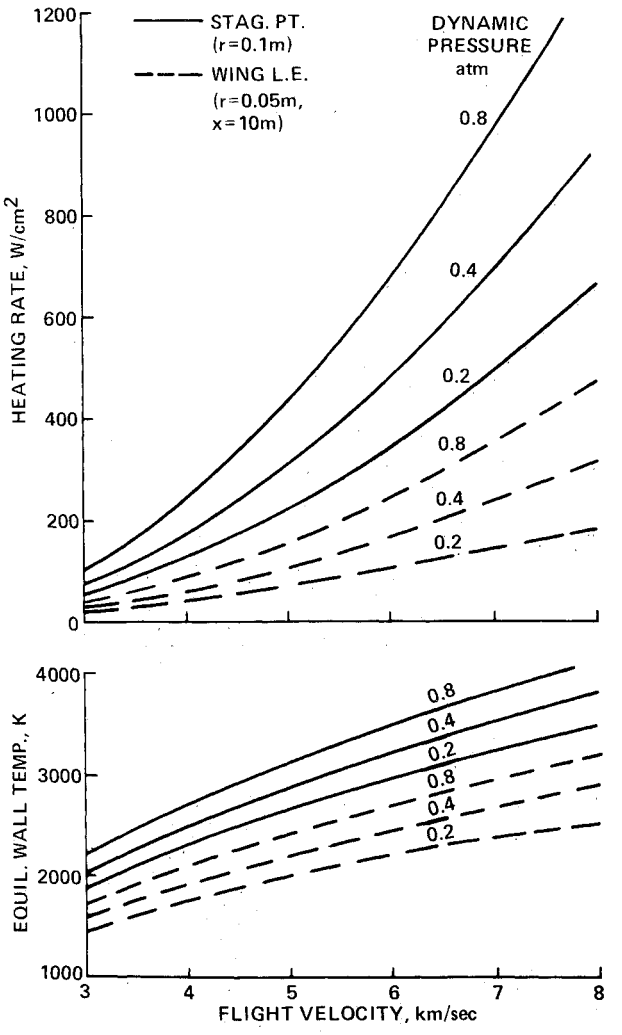

Fig. 6 Ascent heating.

Heating Rates

The three ascent flight paths are characterized by constant dynamic pressures of 0.2, 0.4, and 0.8 atm. The heating rate at the stagnation point and wing leading edge and the corresponding equilibrium wall temperatures are shown in Fig. 6 as a function of velocity. (The location of the leading-edge point is 10 m from the wing root measured along the leading edge.) The steep pressure gradients resulting from small radii of curvature (compared to Shuttle, for example) produce severe heating. The heating rates at the stagnation point range from 660 to over 1200 W/cm^2 at 8 km/s. The corresponding wall temperatures vary from about 3000 to over 4000 K and are far beyond the radiative cooling capabilities of existing, nonablating, heat shield materials. Even the point on the wing leading edge experiences heating rates of 180 to 470 W/cm^2, resulting in wall temperatures of 2500–3200 K. Therefore, both the stagnation point region and the wing leading edge may require some form of active cooling such as ablation or transpiration. (During entry, the peak temperatures at the stagnation point and wing leading edge are 1000–1500 K lower.[1]) The high heating at the leading edge, despite the assumed large sweepback angle of 75 deg, is partly due to turbulence. (In fact, the large sweep angle produces strong crossflow that promotes boundary-layer transition.[19]) The effect of turbulent boundary-layer heating can be seen in Fig. 7, where the heating rates and equilibrium wall temperatures along the hypothetical leading edge are shown at flight speeds of 4, 6, and 8 km/s. Note that the heating along the surface nearly doubles with distance and can reach 500 W/cm^2 at orbital speed. At 8 km/s, the peak wall temperatures are 2700, 3000, and 3300 K for $q = 0.2$, 0.4, and 0.8 atm, respectively.

While the stagnation point region and wing leading edge experience such severe heating that active cooling may be mandatory, large areas of the vehicle surface are exposed to more moderate heating. This can be seen in Fig. 8 where the vehicle's windward centerline heating and temperatures are shown again at speeds up to nearly 8 km/s and for all three trajectories, at points 4 and 10 m from the nose. Despite strong turbulent heating below about 5 km/s, the temperatures peak at about 1500 K, or not much higher than during entry,[1] which is sufficiently low to permit radiative cooling. In fact, the maximum heating rates are nearly the

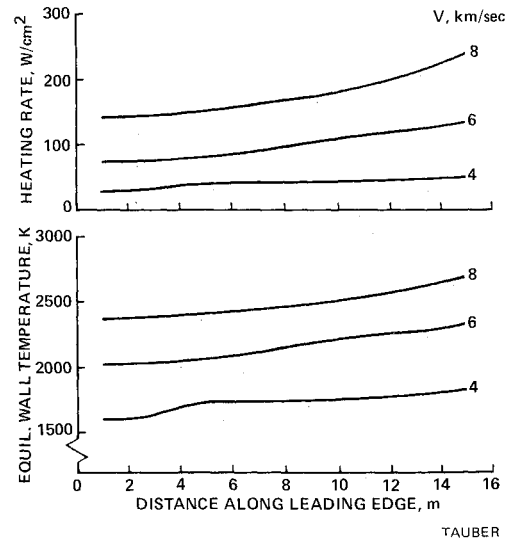

Fig. 7a Wing leading-edge heating; dynamic pressure = 0.2 atm.

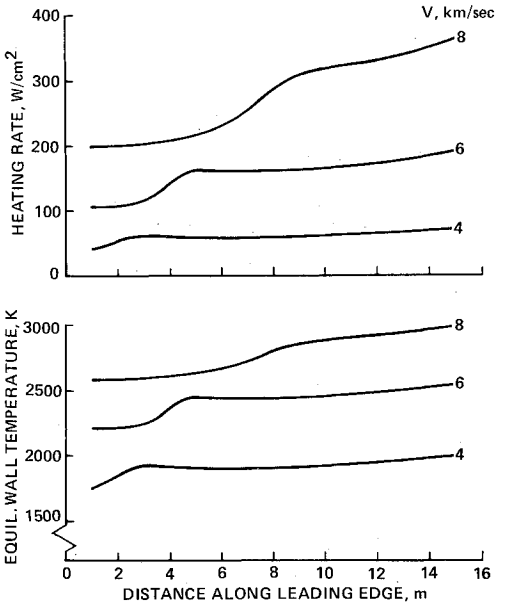

Fig. 7b Wing leading-edge heating; dynamic pressure = 0.4 atm.

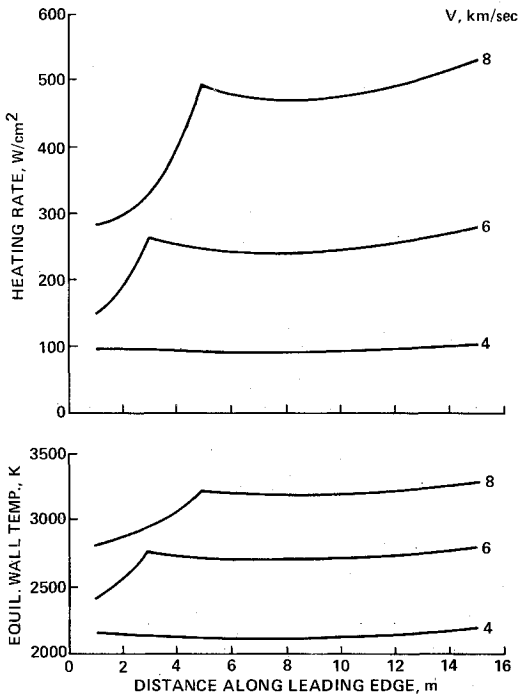

Fig. 7c Wing leading-edge heating; dynamic pressure = 0.8 atm.

same for all three trajectories, because the angle of attack decreases with increasing dynamic pressure. (Note that as flight speed increases the boundary layer becomes laminar. The relaminarization is due to the combination of increasing boundary-layer edge Mach number and decreasing Reynolds number, since Reynolds number is inversely proportional to velocity at constant dynamic pressure.)

Total Heat Loads

The total heating loads at the stagnation point and wing leading edge are shown in Fig. 9 as a function of average acceleration. As expected, the total heating declines

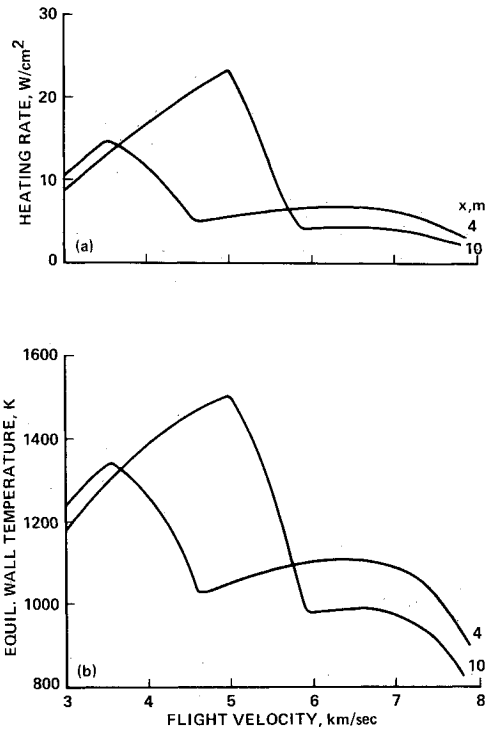

Fig. 8a Body centerline heating during ascent; dynamic pressure = 0.2 atm.

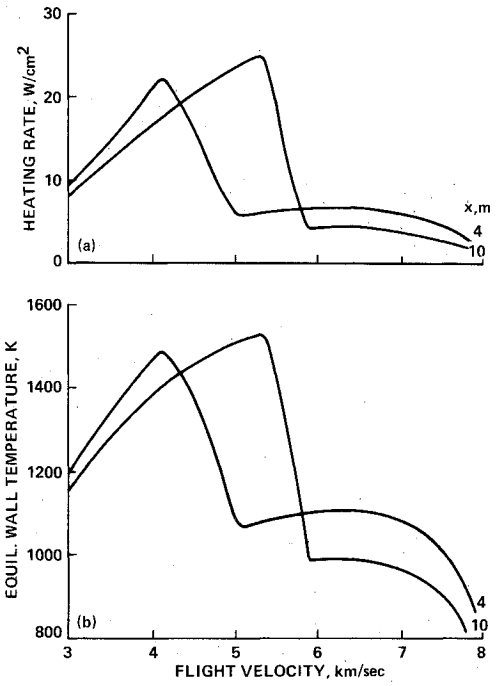

Fig. 8b Body centerline heating during ascent; dynamic pressure = 0.4 atm.

dramatically with increasing acceleration since the duration of the heating pulse decreases. Since the heating load is inversely proportional to the average acceleration [Eq. (19)], the stagnation point total heating decreases from over 1.4 MJ/cm^2 at 0.2 g to about 380 kJ/cm^2 at 0.8 g. The leading-edge total heat loads are roughly one-third of the stagnation point values. The distributions of centerline total heat loads during ascent are shown in Fig. 10 for an average acceleration of 0.2 g. [The heat loads for any other average acceleration can be easily calculated by inverse ratioing of the

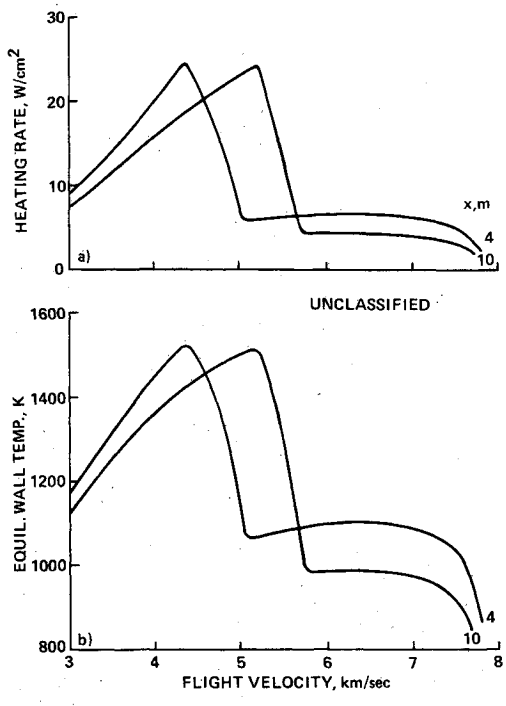

Fig. 8c Body centerline heating during ascent; dynamic pressure = 0.8 atm.

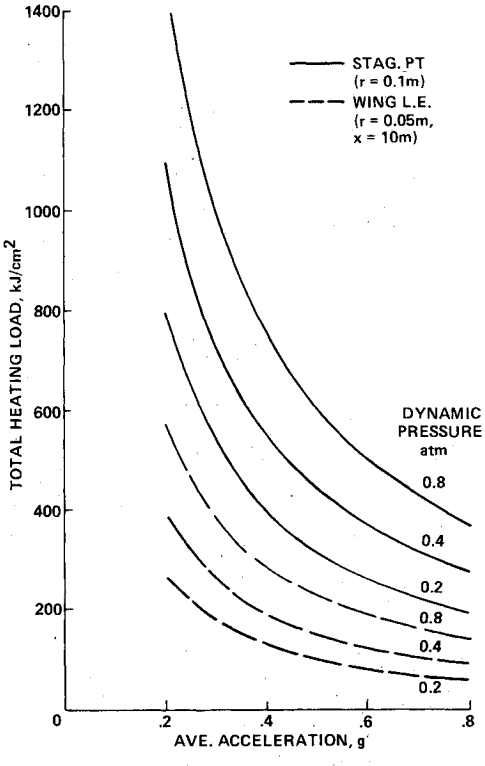

Fig. 9 Ascent total heat loads.

accelerations, Eq. (19).] As already indicated in Fig. 8, the windward centerline heating is weakly dependent on the ascent trajectory. The ascent heat loads average 25–30 kJ/cm², for an acceleration of 0.2 *g*. Most of the heating results from turbulent boundary-layer convection.

In contrast with past experience, the heating environment encountered by the TAV upon atmospheric entry is usually more benign than during ascent. The heat load distributions for entry trajectories having lift/drag ratios of 1.2 and 1.8 are also shown in Fig. 10 for comparison. The high *L/D* trajectory corresponds to a long downrange entry, and the vehicle experiences more than twice the heating of the lower *L/D* case. (A higher *L/D* requires a lower angle of attack; therefore, the drag is less and the entry time longer.) The total heating for both entries is far below the ascent cases, except near the nose. For comparison, one point from Shuttle flight no. 2^{20} is also shown; it falls between the two TAV entry cases.

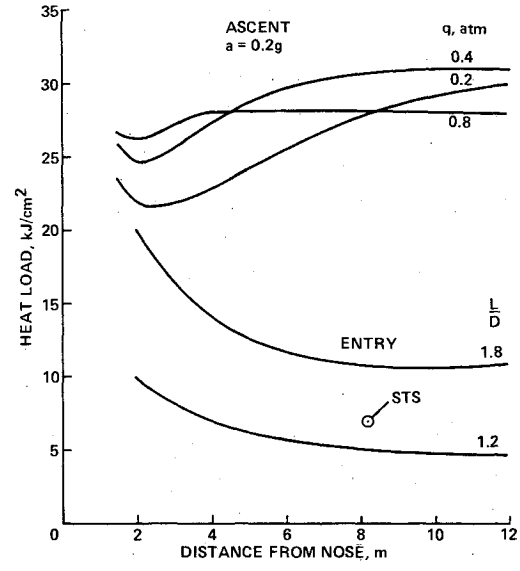

Fig. 10 Total heat loads on centerline.

Ascent heat loads for the stagnation point and wing leading edge depend strongly on the trajectory and are high. The stagnation point value exceeds 1 MJ/cm² and the leading-edge value 0.5 MJ/cm² for an average acceleration of 0.2 *g*. In comparison, the windward centerline ascent heat loads are about 30 kJ/cm² and are relatively insensitive to the dynamic pressure of the trajectory. The entry heat loads are much lower, but more sensitive to the flightpath.

Conclusions

A TAV using primarily airbreathing propulsion must fly in the denser part of the atmosphere to achieve adequate acceleration to reach orbital speed. The elements of a very severe aerothermodynamic environment are, therefore, coupled with the requirement of low aerodynamic drag. To achieve low drag, the vehicle must be slender and must have a relatively sharp nose and wing leading edges. The combination of high heating rates experienced by surfaces with small curvatures and the long ascent times results in severe heating and large total heat loads. The ascent peak stagnation point and wing leading edge equilibrium wall temperatures can reach values of 4000 and 3000 K, respectively, for high-dynamic-pressure trajectories. Therefore, some form of active cooling may be required for these regions of the vehicle. (The corresponding temperatures during entry are about 1500 K lower.) The vehicle's windward centerline temperatures are more moderate, however, with values peaking around 1500 K. Therefore, radiative cooling should be effective over large areas of the vehicle. The windward centerline heat loads are relatively insensitive to the dynamic pressure of the ascent trajectory, in contrast to the stagnation point and wing leading edge. The entry heat loads for the windward surface are much lower, but depend strongly on the flight path. The thermal protection of the TAV poses major challenges.

Appendix

Values for the constants in Eq. (15), for a fully catalytic surface, are listed here. The units of heating rate are watts per square centimeter if the velocity is in meters per second and density in kilograms per cubic meter.

Stagnation point:

$$M=3,\ N=0.5,\ C=1.83(10^{-8})r_n^{-1/2}(1-g_w)$$

Laminar flat plate: $M=3.2,\ n=0.5,$

$$C_1=2.53(10^{-9})\ (\cos\theta)^{1/2}(\ \sin\theta)x^{-1/2}(1-g_w)$$

Turbulent flate plate: $N=0.8$

$$V\leq 3962\ \text{m/s},\ M=3.37$$

$$C_2=3.35(10^{-8})(\cos\theta)^{1.78}(\sin\theta)^{1.6}x_T^{-1/5}$$

$$\times\ (T_w/556)^{-1/4}(1-1.11\ g_w)$$

$$V>3962\ \text{m/s},\ \text{M}=3.7$$

$$C_2=2.20(10^{-9})(\cos\theta)^{2.08}(\sin\theta)^{1.6}x_T^{-1/5}(1-1.11\ g_w)$$

References

[1]Tauber, M.E., Menees, G.P., and Adelman, H.G., "Aerothermodynamics of Transatmospheric Vehicles," *Journal of Aircraft,* Vol 24, Sept. 1987, pp. 594–602.

[2]Eggers, A.J., Allen, H.J., and Niece, S.E., "A Comparative Analysis of the Performance of Long-Range Hypervelocity Vehicles," NACA TR-1382, 1958.

[3]Tauber, M.E. and Paterson, J.A., "Trajectory Module of the NASA Ames Research Center Aircraft Synthesis Program ACSYNT," NASA TM-78497, July 1978.

[4]Russell, W.R. (ed.), "Space Shuttle Transportation System —Operational Aerodynamic Data Book," STS85-0118, Sept. 1985.

[5]Shkadov, L.M., Bukhanova, R.S., Illarionov, V.P., "Mechanics of Optimum Three-Dimensional Motion of Aircraft in the Atmosphere (1972)," NASA TT F-777, March 1975.

[6]Tauber, M.E., "Scaling Relations for Heating During Gliding Entry at Parabolic Speed," *AIAA Journal,* Vol. 24, Dec. 1986, pp. 2047–49.

[7]Marvin, J.G. and Deiwert, G.S., "Convective Heat Transfer in Planetary Gases," NASA TR R-224, July 1965.

[8]Hanley, G.M., "Hypervelocity Laminar Convective Flat Plate Heating," *ARS Journal,* Vol. 32, Nov. 1963, pp. 1740–43.

[9]Arthur, P.D., Shultz, H., and Guard, F.L., "Flat Plate Turbulent Heat Transfer at Hypervelocities," *Journal of Spacecraft and Rockets,* Vol. 3, Oct. 1966, pp. 1549–1551.

[10]Rubesin, M.W., "The Effect of Boundary Layer Growth Along Swept-Wing Leading Edges," Vidya Corp., Rept. 4, 1958.

[11]Morkovin, M.V., "Critical Evaluation of Transition from Laminar to Turbulent Shear Layers with Emphasis on Hypersonically Traveling Bodies," AFFDL-TR-68-149, March 1969.

[12]Goodrich, W.D., Derry, S.M., and Bertin, J.J., "Shuttle Orbiter Boundary-Layer Transition at Flight and Wind Tunnel Conditions," *Shuttle Performance: Lesson Learned,* NASA CP-2283, 1983, pp. 753–779.

[13]Throckmorton, D.A., "Benchmark Determination of Shuttle Orbiter Entry Aerodynamic Heat-Transfer Data," *Journal of Spacecraft and Rockets,* Vol. 20, May-June 1983, pp. 219–224.

[14]Shinn, J.L., Moss, J.N., and Simmonds, A.L., "Viscous Shock-Layer Heating Analysis for the Shuttle Windward Plane with Surface Finite Catalytic Recombination Rates," AIAA Paper 82-0842, June 1982.

[15]Kim, M.D., Swaminathan, S., and Lewis, C.D., "Viscous Shock-Layer Predictions of Three-Dimensional Nonequilibrium Flows Past the Space Shuttle at High Angle of Attack," *Shuttle Performance: Lessons Learned,* NASA CP-2283, 1983, pp. 805–825.

[16]Menees, G.P., Tauber, M.E., Wilson, J.T., and Adelman, H.G., "Ascent Aeromaneuvering Capabilities of Transatmospheric Vehicles," AIAA Paper 87-0513, Jan. 1987.

[17]Van Dyke, M.D., "A Study of Hypersonic Small Disturbance Theory," NACA TR-1194, 1954.

[18]Williams, L.J., "Estimated Aerodynamics of All-Body Hypersonic Aircraft Configurations," NASA TM X-2091, March 1981.

[19]Poll, D.I.A., "Boundary Layer Transition on the Windward Face of Space Shuttle During Re-Entry," AIAA Paper 85-0899, June 1985.

[20]Pitts, W.C. and Murbach, M.S., "Flight Measurements of Tile Gap Heating on the Space Shuttle," AIAA Paper 82-0840, June 1982.